Volume 12 | Number 17 | 7 September 2025

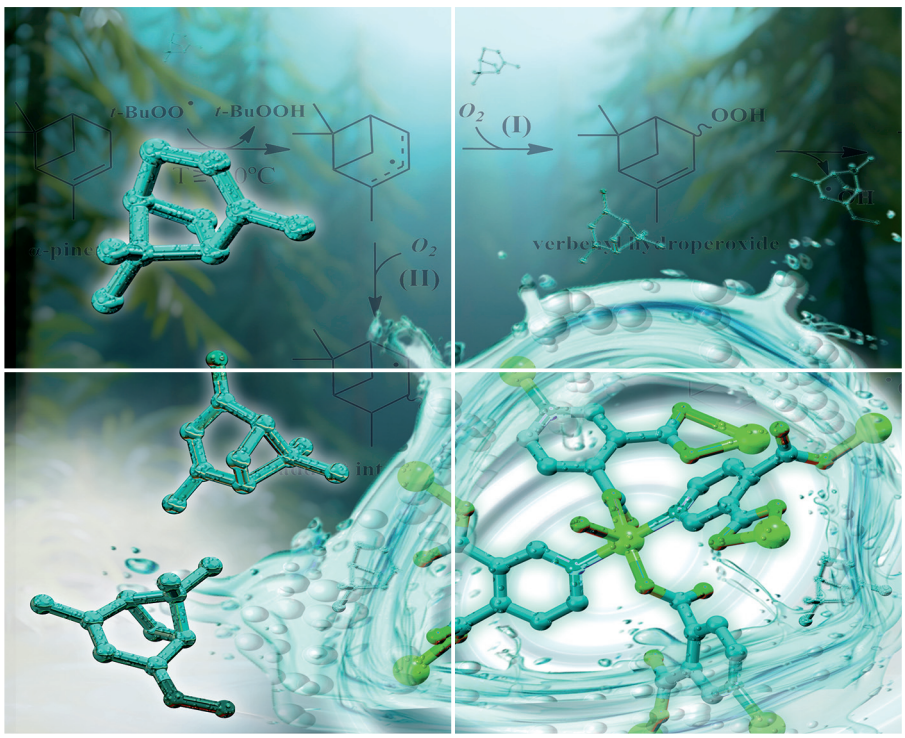

INORGANIC CHEMISTRY

FRONTIERS

CCS 中国化学会 CHINESE CHEMICAL SOCIETY
PEKING UNIVERSITY 1898
ROYAL SOCIETY OF CHEMISTRY
rsc.li/frontiers-inorganic

INORGANIC CHEMISTRY FRONTIERS

RESEARCH ARTICLE

View Article Online
View Journal | View Issue

Cite this: *Inorg. Chem. Front.*, 2025, **12**, 5003

Copper pyridinedicarboxylates: assembly, structures, and catalytic oxidation of terpenes†

Gilvan A. Correia, Chris H. J. Franco, * Marina V. Kirillova * and Alexander M. Kirillov *

Received 20th May 2025,
Accepted 24th June 2025

DOI: 10.1039/d5qi01178g

rsc.li/frontiers-inorganic

Three new copper(II) compounds, formulated as [Cu(pdc)(H_3tea)(H_2O)] (**1**), [Cu_2(μ_3-pdc)$_2$(DMF)(H_2O)$_2$]$_n$·2*n*H_2O (**2**) and [Cu_2(μ_4-pdc)$_2$(H_2O)$_3$]$_n$·3*n*H_2O (**3**), were generated from copper(II) nitrate, 3,4-pyridinedicarboxylic acid (H_2pdc), and triethanolamine (H_3tea). Their crystal structures revealed a discrete 0D complex (**1**) as well as 2D (**2**) and 3D (**3**) coordination polymers (CPs). The obtained compounds were screened as precatalysts for the oxidation of terpenes with molecular oxygen as the oxidizing agent and *t*-BuOOH as the radical initiator. The relationship between the precatalyst structures and the accumulation of α-pinene oxidation products was investigated. Among the three compounds, compound **2** revealed the best activity in α-pinene oxidation. Under the optimized conditions, the conversion of α-pinene reached ~90%, yielding pinene oxide, verbenyl hydroperoxide, verbenol, and verbenone as the main products. Furthermore, compound **2** can catalyze the oxidation of (+)-valencene with O_2 to give (+)-nootkatone. This study showcases the successful synthesis of three new copper-pyridinedicarboxylate derivatives, among which the 2D coordination polymer **2** acts as a particularly efficient precatalyst for upgrading terpenes into value-added oxyfunctionalized products.

10th anniversary statement

For a decade, *Inorganic Chemistry Frontiers* has stood as a leading venue for pioneering research in inorganic chemistry. Serving as both authors and reviewers, we have enjoyed contributing to its remarkable growth. Our laboratory (MINDlab: Molecular Design & Innovation Laboratory) has published several articles that link the molecular design and synthesis of metal complexes & coordination polymers with their catalytic and functional properties. The present study extends this line by presenting new catalysts for the conversion of renewable terpenes into value-added products. Many of these projects arose from collaborations with colleagues in China, showcasing the journal's role to strengthen scientific cooperation between Portugal, China and the global community. We congratulate the editors and all staff on this 10-year milestone and look forward to the discoveries in inorganic chemistry the next decade will unveil.

Introduction

Catalytic oxidation processes are essential for upgrading inexpensive, readily available, and renewable feedstocks, such as terpenic olefins, into valuable oxygen-containing compounds.[1,2] α-Pinene is the most widely available terpene, particularly as a byproduct of the paper and forest industries.[2–4] Its oxidation products, such as verbenol and verbenone, are valuable molecules, as evidenced by their significantly elevated prices relative to α-pinene.[5] The oxygenated derivatives of α-pinene are known for their biologically active properties, such as those exhibited by verbenone (antibacterial, antimicrobial, and anti-inflammatory)[6–8] and verbenol (anti-ischemic and antioxidant).[7,9] Additionally, α-pinene oxide can be used in the synthesis of fragrances.[10] Hence, there is a demand for developing new catalytic systems and protocols for the oxidative functionalization of α-pinene into value-added products.[11,12]

Among the oxidants that can be used for the oxidation of α-pinene, molecular oxygen stands out as the most desirable due to its abundance, low cost, and environmentally friendly nature.[13] Although various studies have been conducted on the oxidation of terpenes with molecular oxygen, many of these processes still face challenges associated with moderate

MINDlab: Molecular Design & Innovation Laboratory, Centro de Química Estrutural, Institute of Molecular Sciences, Departamento de Engenharia Química, Instituto Superior Técnico, Universidade de Lisboa, Av. Rovisco Pais, 1049-001 Lisboa, Portugal. E-mail: chris.franco@tecnico.ulisboa.pt, kirillova@tecnico.ulisboa.pt, kirillov@tecnico.ulisboa.pt

†Electronic supplementary information (ESI) available: Additional data on the synthesis, characterization, and catalytic application of **1–3** (Fig. S1–S35 and Tables S1–S19). CCDC 2389084–2389086. For ESI and crystallographic data in CIF or other electronic format see DOI: https://doi.org/10.1039/d5qi01178g

conversions and/or selectivity,[14–16] as well as the requirement for complex catalytic systems,[17,18] involving precious metals (Pd,[19] V,[20] Ti[21,22]), undesirable organic solvents,[23] high pressures or long reaction times.[24] These factors hinder the development of more sustainable reaction media.

In 2005, Sheldon argued that "the best solvent is no solvent".[25] In this context, added-solvent-free catalytic oxidations of terpenes with molecular oxygen are particularly attractive, especially within the context of green chemistry, aiming to promote the development of more environmentally friendly processes through waste minimization and valorization.[26,27] An interesting oxidation system, using dioxygen as the oxidant and α-pinene as the substrate, was developed on the basis of hierarchically ordered nanostructured MnO_2 as the catalyst.[28] Although this catalyst has shown appealing catalytic behavior in the allylic oxidation of α-pinene to verbenone, the reproducibility of the catalytic synthesis posed some challenges.[28] Another study focused on the oxidation of α-pinene, wherein the impact of the nature of the metal on the product distribution over mesoporous metal–organic frameworks (MIL-101) was emphasized. Chromium-based catalysts favored selectivity to verbenone, while iron catalysts led to the formation of alcohol and peroxide derivatives.[15,16] Despite several examples of added-solvent-free oxidations with dioxygen over different transition-metal catalysts, the application of copper(II)-based catalytic systems for the oxidation of renewable feedstocks such as terpenes, and particularly α-pinene, remains limited.

Given the inherent nature of copper ions and their influence on the oxidation of hydrocarbon substrates,[29–42] motivation has been growing for utilizing this inexpensive, biorelevant, and redox-active transition metal in catalysis.[26,43,44] The field of copper coordination chemistry has seen significant advancements,[45] largely attributed to the widespread use of copper complexes and coordination polymers (CPs) in catalytic systems.[34–42] A wide diversity of copper(II) coordination compounds can be produced by combining a metal source, a carboxylate ligand,[46–48] and an amino alcohol chelator.[40,49–51] Overall, the use of copper(II)-based catalytic systems for the oxidation of α-pinene, with molecular oxygen as the primary oxidizing agent, can be considered a sustainable approach.[22]

Following the above discussion, the main goals of the present study are the synthesis of new copper(II) coordination compounds and their application as precatalysts in the added-solvent-free oxidation of α-pinene with dioxygen as the main oxidant and *t*-BuOOH as the radical initiator. Three new copper-based coordination compounds, $[Cu(pdc)(H_3tea)(H_2O)]$ (**1**), $[Cu_2(\mu_3\text{-}pdc)_2(DMF)(H_2O)_2]_n{\cdot}2nH_2O$ (**2**) and $[Cu_2(\mu_4\text{-}pdc)_2(H_2O)_3]_n{\cdot}3nH_2O$ (**3**), were thus generated from similar reaction systems composed of copper(II) ions and 3,4-pyridinedicarboxylic acid (H_2pdc) as the linker ligand, but under different conditions, namely, reflux, solvothermal treatment, and room-temperature self-assembly with distinct crystallization mediators (triethanolamine, dimethylformamide (DMF) and DL-2-amino-1-butanol, respectively).[52,53] One of the objectives of this work was to explore the assembly of structurally different products from the systems containing copper(II) ions and 3,4-pyridinedicarboxylic acid as the main building blocks. The particular interest in H_2pdc is explained by its coordination versatility and its potential to promote hydrocarbon oxidation reactions. A detailed description of the synthesis, characterization, structural features, and catalytic behavior of the obtained copper(II) compounds is given below.

Experimental

General synthetic procedure for 1–3

In all the syntheses, 3,4-pyridinedicarboxylic acid (H_2pdc; 0.5 mmol, 83 mg) was dissolved in water (5 mL), followed by the addition of aqueous NH_4OH (4 mmol, 1 mL, 4 M) to produce reaction solution A (Fig. 1). In parallel, solution B was prepared by mixing an aqueous solution of $Cu(NO_3)_2{\cdot}3H_2O$ (1.0 mmol, 1.0 mL, 1 M) with different mediators of crystallization, namely,

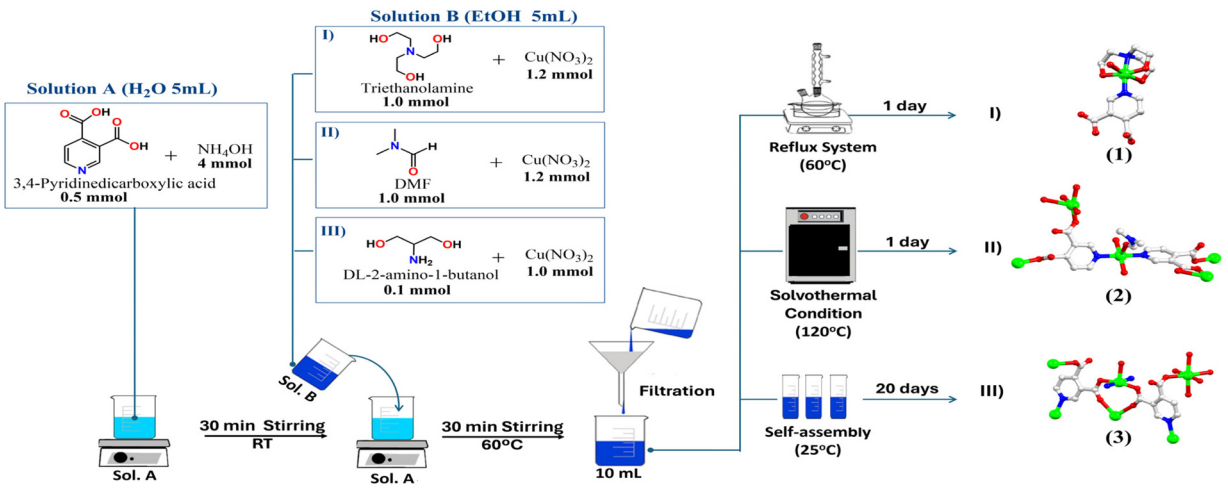

Fig. 1 Schematic representation of the syntheses of **1–3**.

triethanolamine (H_3tea, 1 mmol, 149 mg) for **1**; dimethylformamide (DMF, 1 mmol, 73 mg) for **2**; and DL-2-amino-1-butanol (0.1 mmol, 8.92 mg) for **3**. In all cases, solution B was stirred for 15 min and transferred to solution A under constant stirring for 30 min at 60 °C. This final reaction mixture was filtered to remove any undissolved species and subjected to different methods of crystallization. For **1**, the resulting reaction mixture was subjected to reflux for 12 h at 60 °C. For **2**, the reaction mixture underwent solvothermal conditioning for 24 h at 120 °C, with a cooling rate of 20 °C h^{-1}. Finally, for **3**, the mixture was transferred into several glass vials that were kept open to the air allowing for slow evaporation at room temperature (Fig. 1). Blue crystals of compounds **1** and **2** were formed within 12 h after the experiments, resulting in 70–80% and 75–85% yields based on copper(II) nitrate, respectively. However, the formation of bright blue crystals of **3** required a longer time (20 days) and led to a low product yield (5% based on copper(II) nitrate). These different crystallization methods were employed to obtain a diverse set of self-assembled copper(II) coordination compounds with varied structures, stability, and properties.

We also found an interesting correlation between the use of triethanolamine (in the synthesis of **1**) or DMF (in the synthesis of **2**) and the final yields of products. Higher amounts of these reagents led to increased product yields. For example, doubling the amounts of H_3tea and DMF from 1 to 2 mmol, resulted in ~10% superior yields of **1** and **2**. Unfortunately, our attempts to optimize the yield of compound **3** were not successful.

Analytical data: [Cu(pdc)(H_3tea)(H_2O)] (**1**), calculated for $CuC_{13}H_{20}N_2O_8$ (MW 395.85): C, 39.40%; H, 4.90%; N, 7.07%. Found: C, 39.37%; H, 5.00%; N, 7.01%. TGA (450 °C): formation of CuO (remaining sample weight: exp. 19.0%, calcd 19.3%). FTIR-ATR (KBr, cm^{-1}): 3250 (m br) ν(OH/H_2O), 2920 (w) ν(CH), 1591 (m) ν_{as}(COO), 1483 (w) ν_s(COO), 1382 (s), 1168 (w), 1045 (m), 873 (w), 700 (w). $[Cu_2(\mu_3\text{-pdc})_2(DMF)(H_2O)_2]_n{\cdot}2nH_2O$ (**2**), calculated for $Cu_2C_{17}H_{21}N_3O_{14}$ (MW 600.43): C, 33.88%; H, 4.50%; N, 6.67%. Found: C, 33.84%; H, 4.28%; N, 6.86%. TGA (450 °C): formation of 2CuO (remaining sample weight: exp. 24.7%, calcd 25.1%). FTIR-ATR (KBr, cm^{-1}): 3454 (m br) ν(OH/H_2O), 2828 (w) ν(CH), 1652 (s) ν(C=O), 1620 (s) ν_{as}(COO), 1483 (w), 1394 (w) ν_s(COO), 1278 (s), 839 (w), 688 (w). $[Cu_2(\mu_4\text{-pdc})_2(H_2O)_3]_n{\cdot}3nH_2O$ (**3**), calculated for $Cu_2C_{14}H_{18}N_2O_{14}$ (MW 573.32): C, 29.30%; H, 3.83%; N, 4.88%. Found: C, 29.50%; H, 3.74%; N, 4.87%. FTIR-ATR (cm^{-1}): 3493 (m br) ν(OH/H_2O), 2874 (w) ν(CH), 1631 (m), 1551 (s) ν_{as}(COO), 1483 (w), 1585 (s) 1385 (s) ν_s(COO), 1221 (m) 1029 (w), 904 (w), 717 (w), 522 (m). Additional characterization details are given in the ESI, Fig. S2–S6.†

Single-crystal X-ray diffraction

For compounds **1–3**, suitable, blue-colored single crystals were selected and examined by X-ray diffraction. The data were collected using a Bruker APEX-II CCD diffractometer, using *f* and *w* scans with Mo-Kα radiation (*l* = 0.71073 Å). Data reduction, scaling and absorption corrections were performed with SAINT V8.40B for **1** [54] and CrysAlis PRO for **2** and **3**.[55] The structures of **1–3** were solved using ShelXT 2014/5,[56] ShelXS 2008,[57] and ShelXT 2014/5,[56] respectively. Olex2[58] served as the graphical interface for molecular visualization of structures, while ShelXL 2018/3[59] was employed for computational structure refinement, using full-matrix least-squares minimization on F^2. Compound **2** exhibits twinning, which was addressed by applying a 180-degree rotation around the [001] axis during the refinement process. A BASF twin parameter of 0.385 was included to account for the effects of twinning on the crystal structure. Additionally, compound **3** contains disordered water molecules, which were partially modeled without compromising the overall structural integrity. All non-hydrogen atoms were refined anisotropically. Most of the hydrogen atom positions were calculated geometrically (C–H = 0.87–0.98 Å) and refined using the riding model with U_{iso}(H) = 1.2U_{eq}(C) or 1.5U_{eq}(C) for H atoms bound to O atoms when applicable. X-ray crystallographic details for all compounds are provided in Table 1 (other selected geometric parameters can be found in Tables S1–S6, ESI†). The CCDC codes are 2389084–2389086.†

Powder X-ray diffraction (PXRD)

A D8 Advance diffractometer, which was equipped with a Cu-Kα radiation source (λ = 1.54056 Å) was set to operate at 40 kV and 30 mA, with a nickel filter and a LynxEye linear detector. Diffraction patterns were obtained within a 2θ range of 5° to 50°, employing a standard step size of 0.02° and a counting duration of 0.5 to 1 s for each step with a divergence slit measuring 0.6 mm and primary/secondary Soller slits of 2.5°. To confirm the purity of the microcrystalline products, experimental diffractograms were compared to simulated patterns. Additional details are provided in the ESI (Fig. S7 and S8†).

General procedure for oxidation of terpenes

Initially, 1 mL of substrate (6.30 mmol of α-pinene or 4.50 mmol of (+)-valencene) was placed into a 25 mL round-bottom flask equipped with a reflux condenser, a magnetic stirring bar, and a glass bubbler for oxygen supply from a cylinder. Oxygen flow was controlled *via* apparatus attached to the system, with a typical flow rate of 14 mL min^{-1} (Fig. S13†). Additionally, a minor amount of *t*-BuOOH (TBHP, 70% solution in H_2O, 7.5–30.0 μmol) was added as an initiator along with an appropriate amount of precatalyst (0.035–0.35 mmol). The flask containing all the reagents was immersed in an oil bath and stirred at 800 rpm (20 mm magnetic stirring bar). The reaction was carried out at 60–85 °C for 9 h. Agitation of the reaction mixture was stopped 5 min before collecting the aliquots to ensure that the precatalyst settled at the bottom of the reactor. The aliquots (12 μL) were diluted with acetonitrile (400 μL) and analyzed by gas chromatography (GC) using nitromethane (9 μL) as an internal standard. At the end of the reaction, the resulting solution was centrifuged at 7000 rpm for 2 min. Then, the precatalyst was separated by filtration, washed with ethanol three times and dried at room temperature, followed by powder X-ray diffraction analysis. The yields of verbenyl hydroperoxide were estimated *via* double injection

Table 1 Crystal data and structure refinement details for **1–3**

Compound	**1**	**2**	**3**
Formula	$[Cu(pdc)(H_3tea)(H_2O)]$	$\{[Cu_2(\mu_3\text{-}pdc)_2(DMF)\text{-}(H_2O)_2]_n{\cdot}2nH_2O\}$	$\{[Cu_2(\mu_4\text{-}pdc)_2\text{-}(H_2O)_3]_n{\cdot}3nH_2O\}$
$D_{calc.}$/g cm^{-3}	1.687	1.579	1.751
μ/mm^{-1}	1.450	1.750	2.032
Formula weight	395.85	600.43	573.32
Crystal system	Orthorhombic	Monoclinic	Tetragonal
Space group	*Pca*21	*P*21/*c*	*P*43212
a/Å	14.0769(11)	11.4716(4)	9.5386(1)
b/Å	8.0331(6)	13.2902(4)	9.5386(1)
c/Å	13.7851(11)	16.5985(6)	23.9111(3)
α/°	90	90	90
β/°	90	93.503(3)	90
γ/°	90	90	90
V/Å^3	1558.8(2)	2525.88(15)	2175.55(5)
Z	4	4	4
Radiation type	Mo Kα	Mo Kα	Mo Kα
Measured refl's	19 645	6574	41 124
Indep. Refl's	2935	6574	1998
Refl's $I \geq 2\sigma(I)$	2844	6454	1996
R_{int}	0.023	0.163	0.044
Parameters	221	328	157
Restraints	1	0	0
GoF	1.081	1.210	1.107
wR_2	0.046	0.212	0.235
R_1	0.018	0.076	0.080

of the reaction mixture before and after its treatment with excess triphenylphosphine (PPh_3) to selectively reduce verbenyl hydroperoxide into verbenol.[60–64] All references for the quantitative monitoring of products by GC were confirmed by NMR and/or GC-MS (Fig. S24–S29†). Additional experimental details are given in the ESI.†

Results and discussion

Synthesis and characterization of 1–3

The copper(II) coordination compounds **1–3** were generated using different methods of synthesis and crystallization, namely, reflux, solvothermal treatment, and room-temperature self-assembly, respectively. The reactions were performed in an aqueous ethanol solution using H_2pdc as the main ligand and an excess of $Cu(NO_3)\cdot3H_2O$ (2.4 equivalents). The reaction mixtures also included a crystallization mediator, selected from triethanolamine (H_3tea), dimethylformamide (DMF), or DL-2-amino-1-butanol, as well as a base (aqueous NH_4OH) to maintain the pH value close to 9. The obtained products $[Cu(pdc)(H_3tea)(H_2O)]$ (**1**), $[Cu_2(\mu_3\text{-}pdc)_2(DMF)(H_2O)_2]_n{\cdot}2nH_2O$ (**2**), and $[Cu_2(\mu_4\text{-}pdc)_2(H_2O)_3]_n{\cdot}3nH_2O$ (**3**) were isolated as pure microcrystalline solids and fully characterized by FTIR spectroscopy, elemental and thermal analyses, and powder and single-crystal X-ray diffraction. FTIR-ATR spectroscopic data of **1–3** show typical broad absorption bands at 3600 and 3300 cm^{-1} (Fig. S2–S4†) related to the ν(OH) vibrations of water and OH groups in H_3tea. Strong absorptions at 1591 and 1382 cm^{-1} for **1**, 1620 and 1394 cm^{-1} for **2**, and 1551 and 1385 cm^{-1} for **3** are attributed to ν_{as}(COO) and ν_s(COO) bands of deprotonated and coordinated pdc^{2-} ligands. Additional bands in the 1650–1400 cm^{-1} region correspond to aromatic C–C, C=C and C=N vibrations. There is also an intense ν(C=O) band from DMF in **2** at 1652 cm^{-1}.

Structural description

The structure of $[Cu(pdc)(H_3tea)(H_2O)]$ (**1**) was revealed to be that of a monocopper(II) complex crystallized in an orthorhombic crystal system with the space group $Pca2_1$ (Tables S1 and S2†). The 6-coordinated Cu(II) atom adopts a $\{CuO_4N_2\}$ environment filled by three O atoms from triethanolamine and a terminal H_2O ligand in equatorial sites, while the axial positions are taken by the N atoms from H_3tea and μ-pdc^{2-} (Fig. 2). The latter acts as an N-bound terminal ligand and is totally deprotonated. Despite the distorted octahedral coordination (O_h) environment, the geometry around the copper atom adopts an almost square-based pyramidal configuration, with a geometric parameter τ_5 of 0.04 [d(Cu–O) < 2.5 Å]. This is because the structure clearly exhibits Jahn–Teller distortion, showing elongated bond lengths along the O1–Cu–O4 axis, Cu–O1 [2.316(19) Å] and Cu–O4 [2.525(3) Å], which results in a subgroup pyramidal configuration (C_{4v}).[65–67] This effect causes the amino alcohol arm to arrange itself in a way that creates steric hindrance, restricting access to the copper core, which may serve as a potential catalytic site. The hydrogen bonds in compound **1** contribute 48.7% to the overall stability of the crystallized network. The strongest interaction energies, −222.6 and −164.7 kJ mol^{-1}, are associated mainly with the interactions between the carboxylate groups of pdc^{2-} and the OH functionality of the amino alcohol ligand. The lattice energy ($E_{lattice}$ = −656.2 kJ mol^{-1}), calculated using CrystalExplorer software with B3LYP/6-31G(d,p) wave functions and a 3.8 Å radius, indicates that these relatively strong

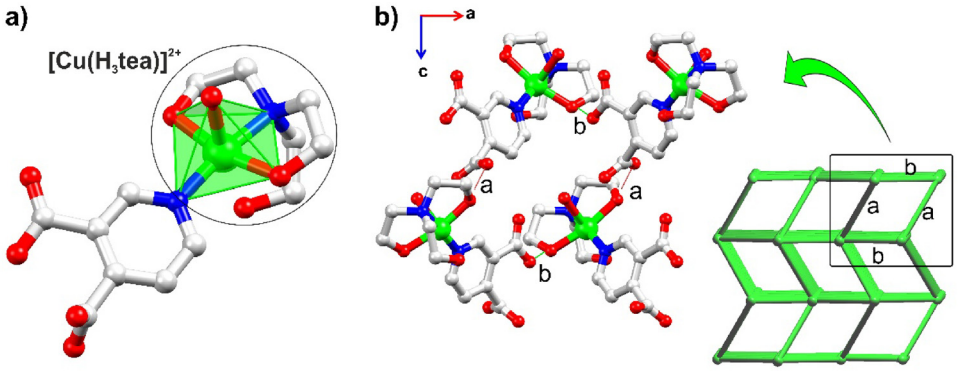

Fig. 2 Crystal structure fragments of compound **1**, [Cu(pdc)(H_3tea)(H_2O)]. (a) Polyhedral representation of the mononuclear copper(II) unit, [Cu(H_3tea)]$^{2+}$. (b) Left: H-bonded motifs a and b; right: simplified representation of crystal packing with the **sqc** topology through H-bonding interactions. Solvent molecules and hydrogen atoms have been omitted for clarity. Color codes: Cu: green; O: red; N: blue; C: gray.

H-bonds play a key role in stabilizing the structure of the compound in the reaction medium (Fig. 2b). A topological approach (ToposPro software[68]) was used to investigate the H-bonds and connectivity of the crystal packing in **1**. It is stabilized by intermolecular O–H···O hydrogen bonds, represented by the *a* and *b* motifs in Fig. 2b, which are the primary interactions within the crystal lattice. Focusing on the strong D–H···A H-bonds [H···A ≤ 2.75 Å, D···A ≤ 3.50 Å, and ∠(D–H···A) > 120°], the resulting H-bonded network is described as a 6-connected uninodal net with a point symbol of ($4^{12}\cdot6^3$), classified within the **sqc** topological type.[69]

The structural analyses of [Cu_2(μ_3-pdc)$_2$(DMF)(H_2O)$_2$]$_n$·2*n*H_2O (**2**) and [Cu_2(μ_4-pdc)$_2$(H_2O)$_3$]$_n$·3*n*H_2O (**3**) reveal polymeric networks with distinct coordination polymer structures. Their type is significantly influenced by the synthetic methodology employed. Compound **2** crystallizes in a centrosymmetric monoclinic system (space group *P*21/*c*), leading to the formation of a two-dimensional (2D) coordination polymer. It features two independent copper coordination units: one displaying an almost ideal square pyramidal arrangement {CuO_3N_2} (τ_5 = 0.09)[70] and the other one exhibiting a distorted square planar geometry {CuO_4} ($\tau_{4'}$ = 0.20 and τ_4 = 0.19)[71] (Fig. 3a). In this structure, the central copper units are cross-linked through μ_3-pdc^{2-} ligands, forming a 2D metal–organic layer with windows of 11.48 × 8.06 Å (Fig. 3b and S10†). However, these potential spaces are occupied by coordinated DMF molecules because of the intercalated crystal packing of the 2D layers along the *bc* plane (Fig. 3c). In contrast, the crystal structure of **3** forms a three-dimensional (3D) CP in a tetragonal crystal system ($P4_32_12$). As in the case of **2**, compound **3** features two distinct copper coordination environments (Fig. 4), but with different geometries: a distorted square pyramidal {CuO_3N_2} (τ_5 = 0.23) environment, (I), and a distorted octahedral {CuO_6} environment, (II). The latter contains four μ_4-pdc^{2-} ligands and two coordinated water molecules. Although DL-2-amino-1-butanol was present in the

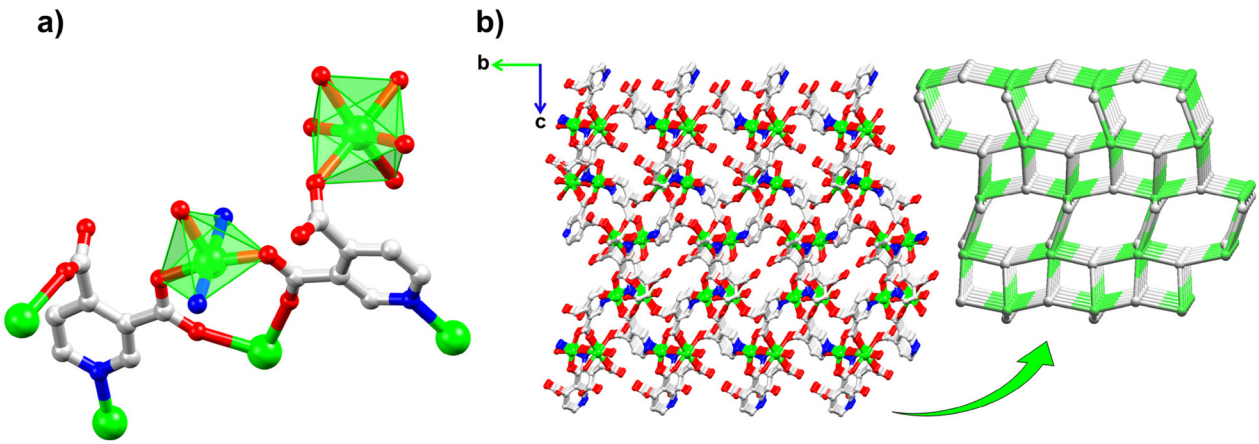

Fig. 3 Crystal structure fragments of **2**, [Cu_2(μ_3-pdc)$_2$(DMF)(H_2O)$_2$]$_n$·2*n*H_2O. (a) Polyhedral representation of mononuclear copper(II) motifs, [Cu(H_2O)$_2$]$^{2+}$ and [Cu(DMF)]$^{2+}$. (b) Right: representation of the 2D metal–organic layer viewed along the *ab* plane. Left: topological representation of the **mcm** network, composed of Cu(II) units (green color) and centroids of μ_3-pdc^{2-} ligands (gray color) (c). Intercalated crystal packing of the 2D layers, viewed down the crystallographic *a*-axis, with spaces occupied by DMF ligands. Solvent molecules and hydrogen atoms have been omitted for clarity. Color codes: Cu: green; O: red; N: blue; C: gray.

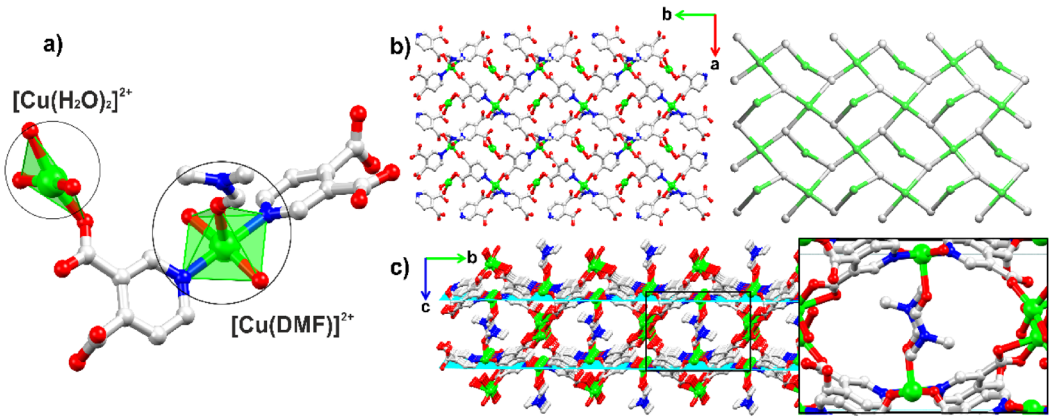

Fig. 4 Crystal structure fragments of compound **3**, $[Cu_2(\mu_4\text{-pdc})_2(H_2O)_3]_n{\cdot}3nH_2O$. (a) Moiety fragment highlighting the copper(II) units, $[Cu(H_2O)_2]^{2+}$ and $[Cu(H_2O)]^{2+}$. (b) Right: representation of the 3D supramolecular arrangement along the *bc* plane, showcasing the 3D network. Left: topological representation of the **ant** network, showing the centroids of the $\{Cu_2(COO)_2\}$ (green) and μ_4-pdc^{2-} (gray) nodes. Water solvent molecules present in the network have been omitted for clarity. Color codes: Cu: green; O: red; N: blue; C: gray.

reaction medium, it does not coordinate to the copper centers. Instead, it functions as a template and assists in the crystallization of **3**. The average bond distances in both CPs are consistent with typical values for such compound types, with d_{avg}(Cu–O) of ~1.99 Å and d_{avg}(Cu–N) of ~2.00 Å (ref. 48) (Tables S5 and S6, ESI†).

Similar to the analysis conducted for **1**, the topological description of **2** and **3** can provide insights into their structural connectivity.[72] The lattice of **2** is constructed from three nodes: μ_3-pdc^{2-}, $[Cu(H_2O)_2]^{2+}$, and $[Cu(DMF)]^{2+}$. However, the $[Cu(H_2O)_2]^{2+}$ moiety was disregarded as it does not contribute to the effective extension or connectivity within the crystal structure of the 2D network. Consequently, the lattice is classified as an **mcm**-type (p4gm) net,[70] defined as a 2-nodal 3,4-connected net with a point symbol of $(5^3)_2(5^4{\cdot}8^2)$, wherein the (5^3) and $(5^4{\cdot}8^2)$ notations correspond to the 3-connected μ_3-pdc^{2-} and 4-connected $[Cu(DMF)]^{2+}$ nodes, respectively.[69] The structure reveals a highly coordinated framework with enhanced exposure of copper centers on the surface. Based on the PXRD data of **2**, it is apparent that the crystallographic faces (011), (002), (202), (20−2), and (221) may play a role in enabling interactions with external molecules acting as substrates (Fig. S9†). Indeed, a surface-colored topological analysis of **2** highlights the efficient distribution of $[Cu(DMF)]^{2+}$ and $[Cu(H_2O)]^{2+}$ centers throughout the network, making this compound promising for applications in catalysis. For compound **3**, the dicopper(II) $\{Cu_2(COO)_2\}$ motifs and μ_4-pdc^{2-} moieties are considered as 6- and 3-connected nodes, respectively, resulting in a binodal 3,6-connected net (Fig. 4b). This network is classified as **ant** (anatase, *I*41/*amd*)[69,73] and has a point symbol of $(4^2{\cdot}6)_2(4^4{\cdot}6^2{\cdot}8^8{\cdot}10)$.

Oxidation of α-pinene

The study of α-pinene oxidation provides a useful model for optimizing the reaction conditions.[14] Hence, the catalytic performance of **1–3** was investigated in an added-solvent-free oxidation of α-pinene in the presence of molecular oxygen and *t*-BuOOH (TBHP) as a radical initiator.[74] The reactions were carried out at 60–85 °C for 9 h, and the main monooxygenated derivatives obtained were verbenone, pinene oxide, and verbenol (Scheme 1). It should be mentioned that compounds **1–3** are not completely intact in the reaction systems containing the oxidant and radical initiator and thus act as precatalysts for copper-based catalytically active species.

The conversion of α-pinene and the accumulation of the main products with time in the presence of **1–3** are shown in Fig. 5. Both **1** and **2** lead to a similar conversion pattern, with ~90% of α-pinene conversion after 9 h. In the reaction with **3**, 80% conversion is achieved under the same conditions. Notably, **2** demonstrates superior catalytic performance, resulting in verbenol, verbenone, and pinene oxide yields of 14%, 23%, and 14%, respectively. Precatalysts **1** and **3** lead to similar yields of verbenol and verbenone (6% and 11%, respectively), while the yields of pinene oxide are in the range of 7.0–9.5%. The slightly inferior performance of these two precatalysts might be related to the lower content of Cu^{2+} in **1** or the reduced availability of copper sites in **3**. The structural characteristics of **1** and **3** may hinder their interaction with terpene molecules, resulting in moderate total product yields (~25%). Unlike its counterparts, compound **2** features a more favorable structure for the catalytic oxidation of α-pinene, resulting in a total product yield of ~51%, which is two-fold

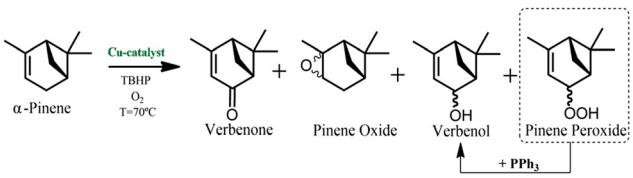

Scheme 1 Schematic representation of α-pinene oxidation in the presence of O_2.

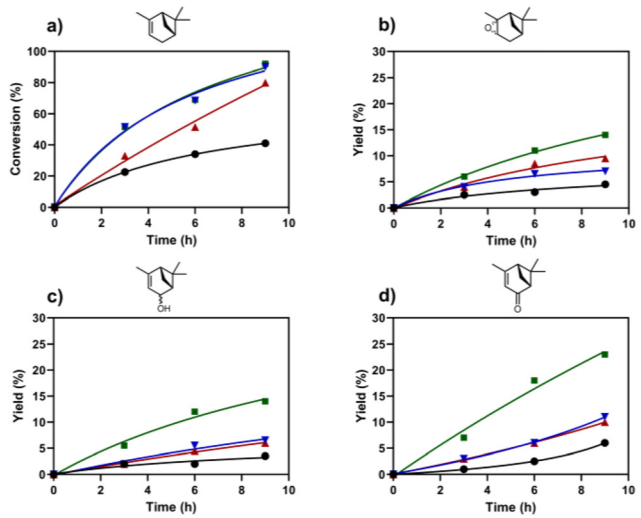

Fig. 5 Oxidation of α-pinene catalyzed by **1** (▼), **2** (■), **3** (▲) and without copper catalyst (●). Conditions: α-pinene (1 mL), catalyst (15 μmol), TBHP (70% aq., 0.35 mmol), 9 h, 800 rpm, 70 °C, O_2 (14 mL min^{-1} = 34.4 mmol h^{-1}). (a) Conversion of α-pinene. Accumulation of monooxygenated derivatives: (b) pinene oxide, (c) verbenol, and (d) verbenone.

higher than those shown by the systems containing **1** and **3**. This superior performance of **2** can be attributed to the presence of Cu^{2+} on the surface of the 2D metal–organic layer (Fig. S9, ESI†) as well as the presence of a labile DMF ligand that can be decoordinated, thereby facilitating the interaction of metal centers with the oxidizing species. Consequently, compound **2** was identified as the most promising precatalyst for further investigation.

To explore the impact of TBHP as a radical initiator in the oxidation of α-pinene, different concentrations of this initiator (0.035 mmol, 0.15 mmol, and 0.35 mmol) were tested in the presence of **2** (15 μmol). Fig. S16† presents an overview of this investigation, demonstrating a similar pattern for the conversion of α-pinene across all concentrations, with 90% conversion after 9 h. However, a higher concentration of TBHP (0.35 mmol) results in better yields of products: 14% pinene oxide, 14% verbenol, and 23% verbenone. At a lower amount of TBHP (0.035 mmol), the yields are inferior (Table S8†).

Aqueous H_2O_2 was also tested as a possible radical initiator for Cu-catalyzed α-pinene oxidation in the presence of O_2. However, the use of H_2O_2 results in a lower total product yield, 20.5% *vs.* 51%, in the presence of the same amount of TBHP (0.35 mmol) (Fig. S17 and Table S9†). No oxidation was observed with O_2 in the absence of any radical initiators and in the presence of the Cu(II) precatalyst.

In the present catalytic system, TBHP was primarily employed as a radical initiator, while molecular oxygen served as the terminal oxidant. The involvement of radical intermediates was also supported by inhibition experiments using TEMPO as a radical scavenger, which led to a significant decrease in catalytic activity (Scheme 2, Fig. S34, and Table S18, ESI†). This indicates that TBHP facilitates the generation of reactive radical species (*e.g.*, *t*-BuO$^{\bullet}$ and *t*-BuOO$^{\bullet}$) essential for initiating the oxidation pathway. However, when the reaction was conducted using TBHP as the single oxidant, only trace amounts of products were formed. Additional experiments under an N_2 atmosphere instead of O_2 were also performed (Fig. S33 and Table S17, ESI†). All these results suggest that the presence of excess molecular oxygen is crucial to sustaining the oxidation process. Therefore, the synergistic use of TBHP and O_2 is necessary.

Fig. S18† provides an overview of the temperature effect on α-pinene oxidation in the presence of **2**. At a higher tempera-

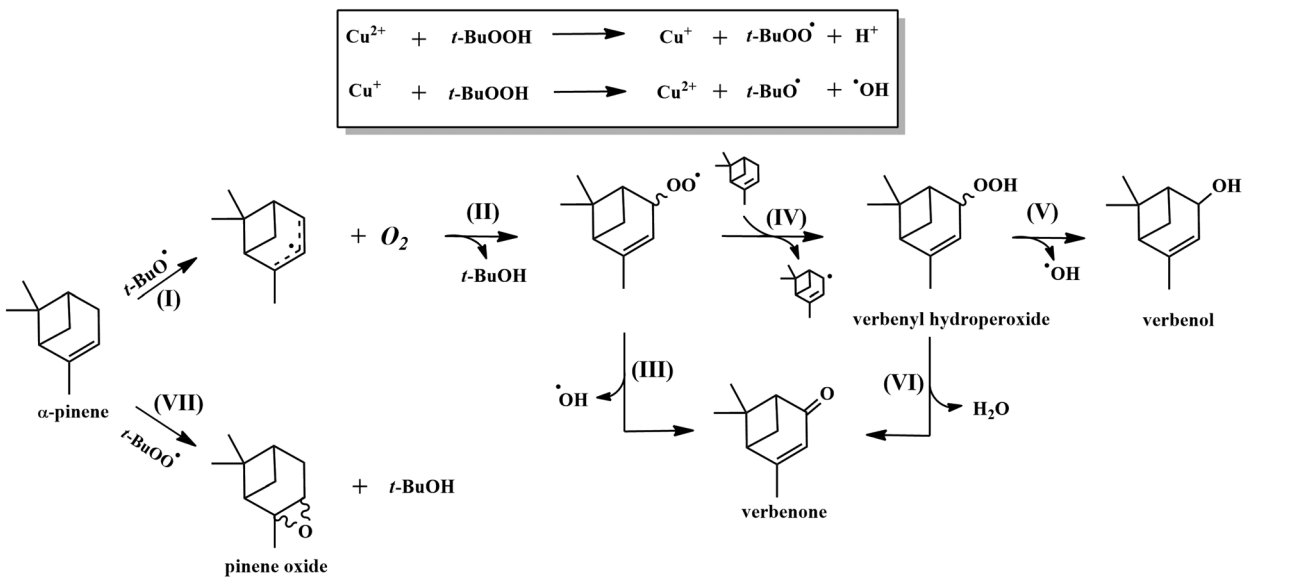

Scheme 2 Mechanistic proposal for the main steps of the allylic oxidation of α-pinene over a Cu-based catalyst using O_2 as the oxidant in the presence of TBHP as the initiator.

ture (85 °C), conversion of α-pinene is almost complete. However, overoxidation occurs after 3 h of the reaction, resulting in the consumption of the formed oxidation products. For example, the yield of pinene oxide decreases from 9 to 0% and that of verbenol drops from 7 to 3% at 85 °C. At a lower temperature (50 °C), the oxidation reaction is slower, leading to α-pinene conversion of 52% and a total yield of the main products of 17% after 9 h. Hence, the optimal reaction temperature of 70 °C provides an advantageous ratio between the conversion (92% after 9 h) and product yield (51%; Table S10†).

Fig. S19† illustrates the effect of precatalyst amounts on the oxidation of α-pinene. An increase of precatalyst **2** loading from 15 to 30 μmol practically does not affect either the reaction rate of α-pinene oxidation or the total product yield (~52–54%). However, at lower precatalyst loading (7.5 μmol), the oxidation is noticeably slower, leading to α-pinene conversion of 78% with a 32.5% total yield of main products (Table S11†). Thus, the optimal amount of **2** was fixed at 15 μmol, which is consistent with previous results.

The effect of the oxygen flow rate on the reaction parameters of α-pinene oxidation in the presence of **2** was analyzed at 8 mL min^{-1} (19.7 mmol h^{-1}) and 14 mL min^{-1} (34.4 mmol h^{-1}). Although good conversion of α-pinene (60% after 9 h) is observed at the oxygen flow rate of 8 mL min^{-1}, the total yield of the main products barely exceeds 17% (Fig. S20†). However, when the reaction medium is saturated with oxygen (O_2 flow rate of 14 mL min^{-1}), higher conversions and product yields are obtained (Table S12†).

To elucidate the reaction mechanism and evaluate the formation of alkyl peroxides (common intermediates in this type of oxidation reaction), a double GC analysis of the reaction aliquots was performed before and after treatment of the reaction mixture with an excess of solid PPh_3. This phosphine is known to selectively reduce alkyl peroxides to alcohols.[60–64] The product distribution (alcohol-to-ketone molar ratio) was then compared (Fig. 6). Due to the thermal instability of verbenyl hydroperoxide under GC conditions, its direct quantification by GC-FID is not possible. Consequently, after treatment of the reaction aliquot with PPh_3, a significant decrease in verbenone

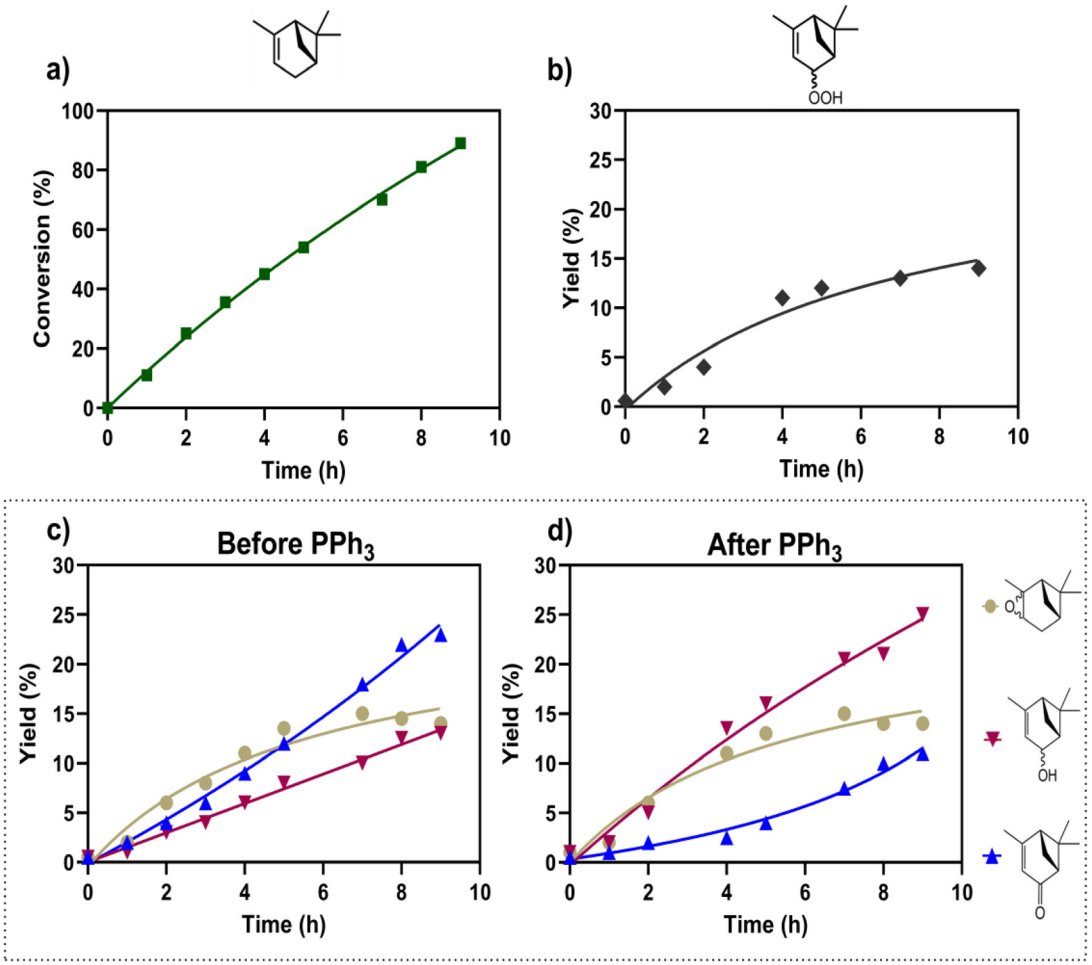

Fig. 6 Oxidation of α-pinene catalyzed by **2**. (a) Conversion of α-pinene. (b) Estimated accumulation of verbenyl hydroperoxide. (c) Accumulation of monooxygenated derivatives before and (d) after addition of PPh_3. Conditions: α-pinene (1 mL), **2** (15 μmol), TBHP (70% in H_2O; 0.35 mmol), 9 h, 800 rpm, temperature (70 °C), and O_2 (14 mL min^{-1}).

yield (from 23 to 11%) and an increase in verbenol yield (from 13% to 25%) were observed, thus permitting the quantity of verbenyl hydroperoxide to be estimated (12% yield; Fig. 6c and d). In addition, the activity of **2**, in terms of turnover frequency (TOF), was approximately 48.5 h^{-1} over the course of the reaction (Table S13†).

At the end of the oxidation reaction, *ca.* 92% of compound **2** can be recovered. Powder X-ray diffraction data revealed a loss of crystallinity in the recovered sample compared to the parent precatalyst **2** (Fig. S30, ESI†). However, FT-IR data indicated that the functional groups remained unchanged relative to the initial measurement with a decrease in the intensity of the ν(C═O) and ν(C–H) bands. This is compelling evidence for the release of the DMF ligand from the Cu-DMF moiety in compound **2** during the recycling of the precatalyst (Fig. S35, ESI†). A recrystallization process of the recovered solid yielded a blue polycrystalline material with the same functional groups as the original compound **2** (Fig. S35, ESI†).

The proposed mechanistic pathway begins with Cu^{2+}-mediated redox routes that convert TBHP into *t*-butoxyl (*t*-BuO$^{\bullet}$) and *t*-butyl peroxyl radicals (*t*-BuOO$^{\bullet}$) (Scheme 2).[75,76] Then, *t*-BuO$^{\bullet}$ abstracts a hydrogen atom from the substrate, generating a resonance-stabilized alkyl radical (**I**).[77] In the presence of molecular oxygen (O_2), this intermediate produces a verbenyl hydroperoxyl species (**II**). The homolytic cleavage of the O–O bond in this species is favored due to its lower energy requirement, producing verbenone (**III**).[77] Additionally, peroxyl radicals can react with the substrate and regenerate the pinene radical, forming verbenyl hydroperoxide (**IV**).[78] This intermediate can either eliminate an HO$^{\bullet}$ radical, leading to the formation of verbenol (**V**) or undergo reduction to verbenone (**VI**).[79] In a parallel pathway, *t*-BuOO$^{\bullet}$ can be added to the C═C bond and generate pinene oxide (**VII**).[77,78]

In the present oxidation, a number of side products can also form as a result of parallel isomerization and polymerization[80,81] reactions that occur in particular after prolonged reaction times and at higher temperatures. Therefore, to evaluate the catalytic properties of **2**, we focused on the accumulation of monooxygenated derivatives (verbenol, verbenone, and pinene oxide).

To experimentally validate this radical mechanism, TEMPO (2,2,6,6-tetramethylpiperidin-1-yl)oxyl was employed as a radical scavenger in the Cu-catalyzed oxidation of α-pinene. In the presence of TEMPO, the yields of the main products drop significantly, corroborating the role of *t*-BuO$^{\bullet}$ and *t*-BuOO$^{\bullet}$ in the oxidation of α-pinene by O_2 (Fig. S34 and Table S18, ESI†).

Additionally, to probe the substrate scope of precatalyst **2**, (+)-valencene was investigated as an alternative terpene substrate under the previously optimized reaction conditions (Scheme 3).

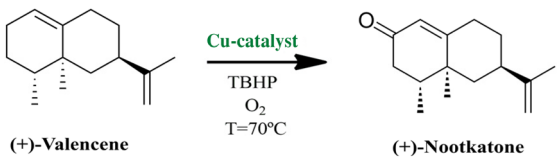

Scheme 3 Schematic representation of (+)-valencene oxidation.

Hence, in the presence of **2**, 71% of (+)-valencene can be converted, yielding 25% of (+)-nootkatone after 9 h of reaction. In contrast, in the blank test without the copper precatalyst, the conversion of (+)-valencene is only 35% to give (+)-nootkatone in a lower yield (11%). This product was isolated from the reaction medium and its formation was confirmed by NMR spectroscopy (^{1}H, 2D HSQC) and GC-MS, the results of which are in accordance with the literature data (Fig. S24–S26†).[82,83] The treatment of the final reaction mixture by PPh_3 does not result in the reduction of the (+)-nootkatone yield, which contrasts with a similar experiment performed for the oxidation of α-pinene. This indicates that (+)-valencene hydroperoxide is not present in the reaction medium (Table S14†).

Conclusions

In summary, this work presents the successful synthesis and structural characterization of three new coordination compounds, namely, a monocopper(II) complex [Cu(pdc)(H_3tea)(H_2O)] (**1**) as well as 2D $[Cu_2(\mu_3\text{-pdc})_2(DMF)(H_2O)_2]_n{\cdot}2nH_2O$ (**2**) and 3D $[Cu_2(\mu_4\text{-pdc})_2(H_2O)_3]_n{\cdot}3nH_2O$ (**3**) coordination polymers. The study further explored the application of 3,4-pyridinedicarboxylic acid (H_2pdc) as a versatile ligand and linker in the molecular design of new copper(II) derivatives.

The copper(II) compounds **1–3** were also investigated as precatalysts in the added-solvent-free oxidation of α-pinene, using molecular oxygen as the oxidant and *t*-BuOOH as the radical initiator. Among the three copper(II) compounds tested, precatalyst **2** exhibited the highest activity in the oxidation of α-pinene (TOF ~ 48.5 h^{-1}). Under optimized conditions, the conversion of α-pinene reached 90%, yielding monooxygenated pinene derivatives (verbenol, verbenone, and pinene oxide) and verbenyl hydroperoxide. Additionally, compound **2** can also act as a precatalyst in the oxidation of (+)-valencene with O_2.

The structural arrangement of **2** features well-dispersed copper moieties across its metal–organic layer, thus potentially facilitating interactions of the metal centers with substrate molecules and enabling the transformation of terpenes into valuable oxyfunctionalized compounds. The synthesis, application and recrystallization of compound **2** may serve as a basis for designing related types of coordination polymers with relevance in oxidation catalysis.

One of the goals of this study was to explore the assembly of structurally different products from the systems containing copper(II) ions and 3,4-pyridinedicarboxylic acid as the main building blocks. A particular interest in this pyridinedicarboxylic acid is governed by its coordination versatility and potential to promote hydrocarbon oxidation reactions, as previously described for related types of N-heteroaromatic carboxylic acids.[84]

The present study should be considered as an initial exploration of the obtained copper(II) coordination compounds

in the catalytic oxidation of terpenes under mild conditions. Compounds **1–3** are not completely intact in the reaction systems containing oxidants and radical initiators and thus act as precatalysts for copper-based catalytically active species.[85] Detailed identification and characterization of these species were outside the scope of the present study and will be investigated in detail by theoretical methods in future research. This work aims to motivate further exploration of added-solvent-free oxidation of terpenes, using catalytic systems based on inexpensive and readily available first-row transition metals.

Conflicts of interest

There are no conflicts to declare.

Data availability

The data supporting this article have been included as part of the ESI.†

Acknowledgements

This project has received funding from the EU *via* its Horizon 2020 research and innovation programme under Grant Agreement No. 860762 (CHAIR project). We also thank the Foundation for Science and Technology (FCT, Portugal; PTDC/QUI-QIN/3898/2020, UIDB/00100/2020, UIDP/00100/2020, LA/P/0056/2020, and UID/00100/2023). C. H. J. Franco acknowledges the research contracts within the PTDC/QUI-QIN/29697/2017 and PTDC/QUI-QIN/3898/2020 projects (2021-2024). We acknowledge the MINDlab: Molecular Design & Innovation Laboratory (MINDlab.pt) at CQE-IST for research facilities.

References

1 M. Lapuerta, I. Tobío-Pérez, M. Ortiz-Alvarez, D. Donoso, L. Canoira and R. Piloto-Rodríguez, Heterogeneous catalytic conversion of terpenes into biofuels: an open pathway to sustainable fuels, *Energies*, 2023, **16**, 2526.
2 N. Semmar, in *Secondary Metabolites in Plant Stress Adaptation: Analytic Space of Secondary Metabolites*, Springer, 2024, pp. 71–109.
3 M. M. Karimkhani, M. Nasrollahzadeh, M. Maham, A. Jamshidi, M. S. Kharazmi, D. Dehnad and S. M. Jafari, Extraction and purification of α-pinene; a comprehensive review, *Crit. Rev. Food Sci. Nutr.*, 2024, **64**, 4286–4311.
4 B. Salehi, S. Upadhyay, I. Erdogan Orhan, A. Kumar Jugran, S. LD Jayaweera, D. A. Dias, F. Sharopov, Y. Taheri, N. Martins and N. Baghalpour, Therapeutic potential of α-and β-pinene: A miracle gift of nature, *Biomolecules*, 2019, **9**, 738.
5 D. R. Naikwadi, S. Dabas, K. Ravi, A. S. Singh, J. H. Advani, S. Subramanian and A. V. Biradar, Recent advances and challenges in the valorization of α–pinene toward value–added chemicals, *Adv. Sustainable Syst.*, 2023, **7**, 2300157.
6 H. E. González-Velasco, M. S. Pérez-Gutiérrez, Á. J. Alonso-Castro, J. R. Zapata-Morales, P. d. C. Niño-Moreno, N. Campos-Xolalpa and M. M. González-Chávez, Anti-inflammatory and antinociceptive activities of the essential oil of tagetes parryi A. Gray (Asteraceae) and verbenone, *Molecules*, 2022, **27**, 2612.
7 J. Petrović, V. Kovalenko, A. Svirid, D. Stojković, M. Ivanov and M. Kostić, Individual stereoisomers of verbenol and verbenone express bioactive features, *J. Mol. Struct.*, 2022, **1251**, 131999.
8 I. Oualdi, K. Elfazazi, H. Azzouzi, A. Oussaid and R. Touzani, Chemical composition and antimicrobial properties of Moroccan Mentha pulegium L. essential oil, *Mater. Today: Proc.*, 2023, **72**, 3768–3774.
9 B. K. Banik, B. M. Sahoo and A. T. Tiwari, *Terpenoids: Chemistry, Biochemistry, Medicinal Effects, Ethno-pharmacology*, 2022, p. 632.
10 S. Leveneur, P. Tolvanen and V. Russo, Catalytic epoxidation reaction, *Catalysts*, 2024, **14**, 285.
11 M. E. Mosquera, G. Jiménez, V. Tabernero, J. Vinueza-Vaca, C. García-Estrada, K. Kosalková, A. Sola-Landa, B. Monje, C. Acosta and R. Alonso, Terpenes and terpenoids: building blocks to produce biopolymers, *Sustainable Chem.*, 2021, **2**, 467–492.
12 M. Winnacker, Pinenes: abundant and renewable building blocks for a variety of sustainable polymers, *Angew. Chem., Int. Ed.*, 2018, **57**, 14362–14371.
13 U. J. Etim, P. Bai, O. M. Gazit and Z. Zhong, Low-temperature heterogeneous oxidation catalysis and molecular oxygen activation, *Catal. Rev.*, 2023, **65**, 239–425.
14 L. Menini, M. C. Pereira, L. A. Parreira, J. D. Fabris and E. V. Gusevskaya, Cobalt-and manganese-substituted ferrites as efficient single-site heterogeneous catalysts for aerobic oxidation of monoterpenic alkenes under solvent-free conditions, *J. Catal.*, 2008, **254**, 355–364.
15 I. Y. Skobelev, K. Kovalenko, V. Fedin, A. Sorokin and O. Kholdeeva, Allylic oxidation of alkenes with molecular oxygen catalyzed by porous coordination polymers Fe-MIL-101 and Cr-MIL-101, *Kinet. Catal.*, 2013, **54**, 607–614.
16 I. Y. Skobelev, A. B. Sorokin, K. A. Kovalenko, V. P. Fedin and O. A. Kholdeeva, Solvent-free allylic oxidation of alkenes with O2 mediated by Fe-and Cr-MIL-101, *J. Catal.*, 2013, **298**, 61–69.
17 P. A. Robles-Dutenhefner, K. A. da Silva Rocha, E. M. Sousa and E. V. Gusevskaya, Cobalt-catalyzed oxidation of terpenes: Co-MCM-41 as an efficient shape-selective heterogeneous catalyst for aerobic oxidation of isolongifolene under solvent-free conditions, *J. Catal.*, 2009, **265**, 72–79.
18 P. A. Robles-Dutenhefner, B. B. Brandão, L. F. De Sousa and E. V. Gusevskaya, Solvent-free chromium catalyzed aerobic oxidation of biomass-based alkenes as a route to valuable fragrance compounds, *Appl. Catal., A*, 2011, **399**, 172–178.

19 A. N. Venancio, L. Menini, D. N. Maronde, E. V. Gusevskaya and L. A. Parreira, Palladium catalyzed oxidation of biorenewable β-citronellol and geraniol for the synthesis of polyfunctionalized fragrances, *Mol. Catal.*, 2021, **504**, 111449.
20 A. A. H. Haidar and D. Agustin, Role of organic solvent and influence of oxidant in the oxidation of linalool catalyzed by molybdenum and vanadium complexes, *Tetrahedron Green Chem.*, 2023, **2**, 100029.
21 A. Wróblewska, J. Grzeszczak, P. Miądlicki, K. Kiełbasa, M. Kujbida, A. Kamińska and B. Michalkiewicz, The Studies on α-pinene oxidation over the TS-1. The influence of the temperature, reaction time, titanium and catalyst Content, *Materials*, 2021, **14**, 7799.
22 H. Martínez, J. Neira, Á. A. Amaya, E. A. Páez-Mozo and F. Martínez Ortega, Selective photooxidation of valencene and thymol with nano-TiO2 and O2 as oxidant, *Molecules*, 2023, **28**, 3868.
23 A. E. Harman-Ware, in *Chemical Catalysts for Biomass Upgrading*, 2020, pp. 529–568.
24 L. A. Parreira, L. Menini and E. V. Gusevskaya, Palladium catalyzed oxidation of renewable terpenes with molecular oxygen: oxidation of α-bisabolol under chloride-free conditions, *Catal. Sci. Technol.*, 2014, **4**, 2016–2022.
25 R. A. Sheldon, Green solvents for sustainable organic synthesis: state of the art, *Green Chem.*, 2005, **7**, 267–278.
26 A. Denicourt-Nowicki, M. Rauchdi, M. Ait Ali and A. Roucoux, Catalytic oxidation processes for the upgrading of terpenes: State-of-the-art and future trends, *Catalysts*, 2019, **9**, 893.
27 M. F. M. G. Resul, A. Rehman, A. M. L. Fernández, V. C. Eze and A. P. Harvey, Development of rapid and selective epoxidation of α-pinene using single-step addition of H 2 O 2 in an organic solvent-free process, *J. Mater. Chem. A*, 2021, **11**, 33027–33035.
28 P. Pal, S. K. Pahari, A. K. Giri, S. Pal, H. C. Bajaj and A. B. Panda, Hierarchically order porous lotus shaped nano-structured MnO 2 through MnCO3: chelate mediated growth and shape dependent improved catalytic activity, *J. Mater. Chem. A*, 2013, **1**, 10251–10258.
29 M. Karuppasamy, B. S. Vachan and V. Sridharan, in *Copper in N-Heterocyclic Chemistry*, ed. A. Srivastava, Elsevier, 2021, pp. 249–288.
30 M. Vafaeezadeh, J. Schaumlöffel, A. Lösch, A. De Cuyper and W. R. Thiel, Dinuclear copper complex immobilized on a Janus-type material as an interfacial heterogeneous catalyst for green synthesis, *ACS Appl. Mater. Interfaces*, 2021, **13**, 33091–33101.
31 L. Wang, N. Ma, N. Wu, X. Wang, J. Xin, D. Wang, J. Lin, X. Li and J. Sun, Stable, Efficient, Copper Coordination Polymer-derived heterostructured catalyst for oxygen evolution under pH-universal conditions, *ACS Appl. Mater. Interfaces*, 2021, **13**, 25461–25471.
32 F. Fan, L. Zhao, Q. Zeng, L. Zhang, X. Zhang, T. Wang and Y. Fu, Self-Catalysis Transformation of metal–organic coordination polymers, *ACS Appl. Mater. Interfaces*, 2023, **15**, 37086–37092.
33 Y. Zan, F. Ben Romdhane, A. Miche, C. Méthivier, J.-M. Krafft, C. Jolivalt and J. Reboul, Copper nanoparticles supported on ZIF-8: Comparison of Cu(II) reduction processes and application as benzyl alcohol oxidation catalysts, *ACS Appl. Mater. Interfaces*, 2023, **15**, 38716–38728.
34 A. E. Wendlandt, A. M. Suess and S. S. Stahl, Copper-Catalyzed aerobic oxidative C-H functionalizations: trends and mechanistic insights, *Angew. Chem., Int. Ed.*, 2011, **50**, 11062–11087.
35 A. M. Kirillov, M. V. Kirillova and A. J. L. Pombeiro, in *Advances in Inorganic Chemistry*, ed. R. van Eldik and C. D. Hubbard, Academic Press, 2013, vol. 65, pp. 1–31.
36 A. N. Bilyachenko, M. S. Dronova, A. I. Yalymov, F. Lamaty, X. Bantreil, J. Martinez, C. Bizet, L. S. Shul'pina, A. A. Korlyukov, D. E. Arkhipov, M. M. Levitsky, E. S. Shubina, A. M. Kirillov and G. B. Shul'pin, Cage-like Copper(II) silsesquioxanes: transmetalation reactions and structural, quantum chemical, and catalytic studies, *Chem. – Eur. J.*, 2015, **21**, 8758–8770.
37 E. Loukopoulos, A. Abdul-Sada, G. Csire, C. Kállay, A. Brookfield, G. J. Tizzard, S. J. Coles, I. N. Lykakis and G. E. Kostakis, Copper(II)-benzotriazole coordination compounds in click chemistry: a diagnostic reactivity study, *Dalton Trans.*, 2018, **47**, 10491–10508.
38 J. Gu, M. Wen, Y. Cai, Z. Shi, A. S. Arol, M. V. Kirillova and A. M. Kirillov, Metal–organic architectures assembled from multifunctional polycarboxylates: hydrothermal self-assembly, structures, and catalytic activity in alkane oxidation, *Inorg. Chem.*, 2019, **58**, 2403–2412.
39 A. Hossain, A. Bhattacharyya and O. Reiser, Copper's rapid ascent in visible-light photoredox catalysis, *Science*, 2019, **364**, eaav9713.
40 I. F. M. Costa, M. V. Kirillova, V. André, T. A. Fernandes and A. M. Kirillov, Time-dependent self-assembly of Copper(II) coordination polymers and tetranuclear rings: catalysts for oxidative functionalization of saturated hydrocarbons, *Inorg. Chem.*, 2021, **60**, 14491–14503.
41 L. Marais, H. C. M. Vosloo and A. J. Swarts, Homogeneous oxidative transformations mediated by copper catalyst systems, *Coord. Chem. Rev.*, 2021, **440**, 213958.
42 B. Xu, Q. Xu, Q. Wang, Z. Liu, R. Zhao, D. Li, P. Ma, J. Wang and J. Niu, A Copper-containing polyoxometalate-based Metal–Organic Framework as an efficient catalyst for selective catalytic oxidation of alkylbenzenes, *Inorg. Chem.*, 2021, **60**, 4792–4799.
43 J. R. Ludwig and C. S. Schindler, Catalyst: sustainable catalysis, *Chem*, 2017, **2**, 313–316.
44 H. Wang, Y. Pei, K. Wang, Y. Zuo, M. Wei, J. Xiong, P. Zhang, Z. Chen, N. Shang, D. Zhong and P. Pei, First-row transition metals for catalyzing oxygen redox, *Small*, 2023, **19**, 2304863.
45 K. N. Aziz, K. M. Ahmed, R. A. Omer, A. F. Qader and E. I. Abdulkareem, A review of coordination compounds: structure, stability, and biological significance, *Rev. Inorg. Chem.*, 2024, **45**, 1–19.

46 J. Ai, Y. Zhao and Z. z. Tian, Two novel coordination polymers based on "V"-shaped carboxylic acid: Synthesis, crystal structure and properties, *J. Mol. Struct.*, 2023, **1278**, 134873.
47 Y.-H. Gao, P.-P. Huang, H.-T. Xu, P. Huang, B. Liu, J.-F. Lu and H.-G. Ge, Two novel Zn(II) coordination polymers constructed by the same dicarboxylate and different bis-imidazole as co-ligand: Syntheses, crystal structures and properties, *J. Mol. Struct.*, 2023, **1281**, 135106.
48 Q. Zhang, Y. Wang, Y. Ge, Q. Liu and J.-P. Lang, Regulation of crystal structures and solid-state photoreactivity of diolefin coordination polymers by carboxylate ligands, *Inorg. Chem.*, 2023, **62**, 19080–19086.
49 S. S. P. Dias, M. V. Kirillova, V. André, J. Kłak and A. M. Kirillov, New tetracopper(II) cubane cores driven by a diamino alcohol: self-assembly synthesis, structural and topological features, and magnetic and catalytic oxidation properties, *Inorg. Chem.*, 2015, **54**, 5204–5212.
50 T. A. Fernandes, C. I. M. Santos, V. André, S. S. P. Dias, M. V. Kirillova and A. M. Kirillov, New aqua-soluble dicopper(II) aminoalcoholate cores for mild and water-assisted catalytic oxidation of alkanes, *Catal. Sci. Technol.*, 2016, **6**, 4584–4593.
51 T. A. Fernandes, C. I. M. Santos, V. André, J. Kłak, M. V. Kirillova and A. M. Kirillov, Copper(II) coordination polymers self-assembled from aminoalcohols and pyromellitic acid: Highly active precatalysts for the mild water-promoted oxidation of alkanes, *Inorg. Chem.*, 2016, **55**, 125–135.
52 F. M. Scaldini, C. C. Corrêa, M. I. Yoshida, K. Krambrock and F. C. Machado, 2-D coordination polymers of copper and cobalt with 3,4-pyridinedicarboxylic acid: synthesis, characterization, and crystal structures, *J. Coord. Chem.*, 2014, **67**, 2967–2982.
53 X.-W. Liu, R. Guo, H. Liu, Y.-Q. Yu, X.-W. Qi, J.-Y. Xu and C.-Z. Xie, Two series of novel 3D potentially porous heterometallic Cu–Ln coordination frameworks assembled by 3,4-pyridinedicarboxylic acid with different topologies and channels: syntheses, structures, luminescence and magnetic properties, *RSC Adv.*, 2015, **5**, 15059–15068.
54 *Bruker, Apex 3, v2018.1-0, SAINT V8.40B*, Bruker AXS Inc., Madison, 2018.
55 O. D. Rigaku, *CrysAlis PRO software system, Version*, 2018, **1**, l.
56 G. Sheldrick, MS96.O06, *Acta Crystallogr.*, 2014, **70**, C1437.
57 G. Shelx, Sheldrick, *Acta Crystallogr.*, 2008, **64**, 112–122.
58 O. V. Dolomanov, L. J. Bourhis, R. J. Gildea, J. A. Howard and H. Puschmann, OLEX2: a complete structure solution, refinement and analysis program, *J. Appl. Crystallogr.*, 2009, **42**, 339–341.
59 G. Sheldrick, *SHELXL-2018/3 software package*, University of Göttingen, Germany, 2018.
60 G. B. Shul'pin, Metal-catalyzed hydrocarbon oxygenations in solutions: the dramatic role of additives: a review, *J. Mol. Catal. A: Chem.*, 2002, **189**, 39–66.
61 A. N. Bilyachenko, A. I. Yalymov, L. S. Shul'pina, D. Mandelli, A. A. Korlyukov, A. V. Vologzhanina, M. A. Es'kova, E. S. Shubina, M. M. Levitsky and G. B. Shul'pin, Novel cage-like hexanuclear nickel(II) silsesquioxane. synthesis, structure, and catalytic activity in oxidations with peroxides, *Dalton Trans.*, 2016, **21**, 13663–13666.
62 G. B. Shul'pin, New trends in oxidative functionalization of carbon–hydrogen bonds: A review, *Inorg. Chem.*, 2017, **56**, 15026–15040.
63 A. N. Kulakova, A. N. Bilyachenko, M. M. Levitsky, V. N. Khrustalev, A. A. Korlyukov, Y. V. Zubavichus, P. V. Dorovatovskii, F. Lamaty, X. Bantreil, B. Villemejeanne, J. Martinez, L. S. Shul'pina, E. S. Shubina, E. I. Gutsul, I. A. Mikhailov, N. S. Ikonnikov, U. y. S. Tsareva and G. B. Shul'pin, Si10Cu6N4 Cage hexacoppersilsesquioxanes containing N Ligands: synthesis, structure, and high catalytic activity in peroxide oxidations, *Inorg. Chem.*, 2017, **56**, 15026–15040.
64 A. I. Yalymov, A. N. Bilyachenko, M. M. Levitsky, A. A. Korlyukov, V. N. Khrustalev, L. S. Shul'pina, P. V. Dorovatovskii, M. A. Es'kova, F. Lamaty, X. Bantreil, B. Villemejeanne, J. Martinez, E. S. Shubina, Y. N. Kozlov and G. B. Shul'pin, High catalytic activity of heterometallic (Fe6Na7 and Fe6Na6) cage silsesquioxanes in oxidations with peroxides, *Catalysts*, 2017, **7**, 101.
65 M. A. Halcrow, Jahn–Teller distortions in transition metal compounds, and their importance in functional molecular and inorganic materials, *Chem. Soc. Rev.*, 2013, **42**, 1784–1795.
66 M. A. Halcrow, Interpreting and controlling the structures of six-coordinate copper(II) centres–When is a compression really a compression?, *Dalton Trans.*, 2003, 4375–4384.
67 J. A. de Azevedo-França, E. Barrias, C. H. J. Franco, W. Villarreal, E. G. Vieira, A. M. D. C. Ferreira, W. de Souza and M. Navarro, Promising fluconazole based zinc(II) and copper(II) coordination polymers against Chagas disease, *J. Inorg. Biochem.*, 2022, **233**, 111834.
68 V. A. Blatov, A. P. Shevchenko and D. M. Proserpio, applied topological analysis of crystal structures with the program package ToposPro, *Cryst. Growth Des.*, 2014, **14**, 3576–3586.
69 B. C. Exselent, Reticular Chemistry Structure Resource, **https://rcsr.anu.edu.au/**, (accessed 01-09-2024).
70 A. G. Blackman, E. B. Schenk, R. E. Jelley, E. H. Krenske and L. R. Gahan, Five-coordinate transition metal complexes and the value of τ 5: observations and caveats, *Dalton Trans.*, 2020, **49**, 14798–14806.
71 L. Yang, D. R. Powell and R. P. Houser, Structural variation in copper(I) complexes with pyridylmethylamide ligands: structural analysis with a new four-coordinate geometry index, τ 4, *Dalton Trans.*, 2007, **9**, 955–964.
72 S. R. Batten, N. R. Champness, X.-M. Chen, J. Garcia-Martinez, S. Kitagawa, L. Öhrström, M. O'Keeffe, M. Paik Suh and J. Reedijk, Terminology of metal–organic frameworks and coordination polymers, *Pure Appl. Chem.*, 2013, **85**, 1715–1724.

73 J. M. Verduzco, H. Chung, C. Hu and W. Choe, Metal–Organic Framework assembled from t-shaped and octahedral nodes: a mixed-linker strategy to create a rare anatase TiO2 topology, *Inorg. Chem.*, 2009, **48**, 9060–9062.
74 O. A. Kholdeeva, I. Y. Skobelev, I. D. Ivanchikova, K. A. Kovalenko, V. P. Fedin and A. B. Sorokin, Hydrocarbon oxidation over Fe-and Cr-containing metal-organic frameworks MIL-100 and MIL-101 - a comparative study, *Catal. Today*, 2014, **238**, 54–61.
75 D. Saberi, F. Shojaeyan and K. Niknam, Oxidative self-coupling of aldehydes in the presence of CuCl2/TBHP system: direct access to symmetrical anhydrides, *Tetrahedron Lett.*, 2016, **57**, 566–569.
76 Jyoti, S. Devi, Manisha, D. Wadhwa, J. Sindhu and V. Kumar, TBHP: A sustainable alternative for carbon-oxygen bond formation, *Eur. J. Org. Chem.*, 2024, e202301030.
77 L. J. Zhou, X. H. Liu, H. W. Zhang, C. Xue, H. K. Zhong and X. T. Zhou, Unravelling the different pathways of cyclohexene oxidation via a peroxyl radical generated from tert-butyl hydroperoxide (TBHP) by various metal salts, *Org. Chem. Front.*, 2025, **12**, 48–56.
78 U. Neuenschwander, F. Guignard and I. Hermans, Mechanism of the aerobic oxidation of α–pinene, *ChemSusChem*, 2010, **3**, 75–84.
79 S. N. Xu, A. Draksharapu, W. Rasheed and L. Que, Acid pKa dependence in O-O bond heterolysis of a nonheme FeIII-OOH intermediate to form a potent FeIV═O oxidant with herne compound I-like reactivity, *J. Am. Chem. Soc.*, 2019, **141**, 16093–16107.
80 P. Mäki-Arvela, N. Shcherban, C. Lozachmeur, V. Russo, J. Wärnå and D. Y. Murzin, Isomerization of α-pinene oxide: solvent effects, kinetics and thermodynamics, *Catal. Lett.*, 2019, **149**, 203–214.
81 H. Miyaji, K. Satoh and M. Kamigaito, Bio–Based polyketones by selective ring–opening radical polymerization of α–pinene–derived pinocarvone, *Angew. Chem., Int. Ed.*, 2016, **55**, 1372–1376.
82 T. Wriessnegger, P. Augustin, M. Engleder, E. Leitner, M. Müller, I. Kaluzna, M. Schürmann, D. Mink, G. Zellnig and H. Schwab, Production of the sesquiterpenoid (+)-nootkatone by metabolic engineering of Pichia pastoris, *Metab. Eng.*, 2014, **24**, 18–29.
83 Y. Wang, Y. Kuang and Y. Wang, Rh 2 (esp) 2-catalyzed allylic and benzylic oxidations, *Chem. Commun.*, 2015, **51**, 5852–5855.
84 A. M. Kirillov and G. B. Shul'pin, Pyrazinecarboxylic acid and analogs: highly efficient co-catalysts in the metal-complex-catalyzed oxidation of organic compounds, *Coord. Chem. Rev.*, 2013, **257**, 732–754.
85 D. A. Ruddy, S. E. Habas and R. L. Brutchey, A Note to Reviewers Suggesting Post-Reaction Catalyst Characterization: Know What You're Asking For, *Inorg. Chem.*, 2025, **64**, 3627–3630.